Thermal emission and absorption of radiation in finite inverted-opal photonic crystals

Marian Florescu,[1,*] Hwang Lee,[2] Andrew J. Stimpson,[1] and Jonathan Dowling[2,3]
[1]*Quantum Computing Technologies Group, Jet Propulsion Laboratory, California Institute of Technology, MS 126-347, 4800 Oak Grove Drive, Pasadena, California 91109, USA*
[2]*Hearne Institute for Theoretical Physics, Department of Physics and Astronomy, Louisiana State University, 202 Nicholson Hall, Tower Drive, Baton Rouge, Louisiana 70803, USA*
[3]*Institute for Quantum Studies, Department of Physics, Texas A&M University, College Station, Texas 77843, USA*
(Received 19 November 2004; revised manuscript received 3 June 2005; published 22 September 2005)

We study theoretically the optical properties of a finite inverted-opal photonic crystal. The light-matter interaction is strongly affected by the presence of the three-dimensional photonic crystal and the alterations of the light emission and absorption processes can be used to suppress or enhance the thermal emissivity and absorptivity of the dielectric structure. We investigate the influence of the absorption present in the system on the relevant band edge frequencies that control the optical response of the photonic crystal. Our study reveals that the absorption processes cause spectral broadening and shifting of the band edge optical resonances, and determine a strong reduction of the photonic band gap spectral range. Using the angular and spectral dependence of the band edge frequencies for stop bands along different directions, we argue that by matching the blackbody emission spectrum peak with a prescribed maximum of the absorption coefficient, it is possible to achieve an angle-sensitive enhancement of the thermal emission/absorption of radiation. This result opens a way to realize a frequency-sensitive and angle-sensitive photonic crystal absorbers/emitters.

DOI: 10.1103/PhysRevA.72.033821 PACS number(s): 42.50.Nn, 41.20.Jb, 42.70.Qs, 78.66.Vs

I. INTRODUCTION

Photonic crystals and in particular photonic band gap (PBG) materials constitute a class of dielectric materials in which the basic electromagnetic interaction is controllably altered over certain frequencies and length scales [1–5]. The ability to tailor the optical properties in a prescribed manner and the specific symmetry properties of the electromagnetic field inside a PBG are the fundamental instruments at our disposal to design materials and devices that control the emission and absorption properties of light. In the context of quantum optics, the radiation reservoir associated with a photonic crystal presents drastic departures from the ordinary vacuum case, and strong modifications of the local density of photonic modes give rise to phenomena including the inhibition and enhancement of the spontaneous emission [6], strong localization of light [7], formation of atom-photon bound states [8], quantum interference effects in spontaneous emission [9], single atom and collective atomic switching behavior by coherent resonant pumping, and atomic inversion without fluctuations [10]. These remarkable features have attracted a considerable interest in important technological applications of photonic crystals such as low-threshold microlasers [11,12], ultrafast all-optical switches, and microtransistors [13,14]. Most of the applications of photonic crystals are exploiting the fundamental nonlinear effects facilitated by the photonic band edge that separates the photonic band gap from the continuum of propagating modes.

The modifications of the spontaneous emission rates of atoms or semiconductors embedded in photonic crystal determine, in turn, important alterations of thermal radiative processes. Thermal radiation is just spontaneous emission that is thermally driven and is in thermal equilibrium with its material surroundings. By optimizing the coupling of the multimode radiation field of a PBG material and a spatially extended collection of atomic or electronic emitters, it is possible to achieve dramatic modifications of Planck's blackbody radiation spectrum [15–17]. In the photonic band gap spectral range, the thermal emission of radiation is strongly suppressed, whereas for specific frequencies in the allowed photonic bands that correspond to transmission resonances of the photonic crystal, the thermal emission of radiation is enhanced and reaches the blackbody limit. The ability to control the thermal emission and absorption of radiation in a photonic crystal may find many technological applications in the field of thermally pumped optical devices such as lasers, tunable infrared emitters, or thermovoltaic energy conversion devices.

The electromagnetic properties of infinite photonic crystals have been analyzed in detail. However, the theoretical analysis is typically limited to either nonabsorptive materials [18] or (with some notable exceptions [19,20]) to lower-dimensional absorptive photonic crystals [15,21]. On the other hand, the strong dependence of the stop-gap effect and implicitly of the thermal emissive/absorptive response on the relative orientation with respect to the periodicity direction/plane of the structure in one-dimensional and two-dimensional photonic crystals has inspired successful experimental studies of three-dimensional (3D) structures [22]. In this context, a detailed analysis of the optical properties of an absorbing finite 3D photonic crystal is of particular interest.

In this paper, we investigate the transmission and absorption properties and the thermal emission of a finite sample of inverted-opal photonic crystals, and show that the presence of the absorption processes cause spectral broadening and

*Electronic address: marian.florescu@jpl.nasa.gov

shifting of the band edge optical resonances and determine a strong reduction of the photonic band gap spectral range, and that the finite size character of the photonic crystal sample leads to a stronger dependence these optical response on the propagation direction of the incident radiation. We also evaluate the spectral and angular dependence of the thermal response of the inverted opal structure. The exact knowledge of the angular and spectral dependence of the band edge frequencies can be used to match the blackbody emission spectrum peak with a prescribed maximum of the absorption coefficient. Thus, it is possible to achieve an angle-sensitive enhancement of the thermal emission/absorption of radiation. This result may open a way to realize frequency-sensitive and angle-sensitive photonic crystal absorbers/emitters, which may find applications in thermovoltaic energy conversion devices [23].

This paper is organized as follows. In Sec. II, we introduce the physical system we investigate and present a brief review of the theoretical formalism and numerical approach we use. In Sec. III, we analyze the optical (transmission and absorption coefficients) and thermal (absolute thermal power spectrum) response of a finite inverted opal photonic crystal in different configurations. In Sec. III A, we calculate the transmission spectrum for nonabsorbing inverted opal structures, while in Sec. III B we calculate the absorption and thermal power spectra for an inverted opal structure that contains an absorptive material. In Sec. III C, we consider a different configuration, in which the photonic crystal structure is used as passive filter against the thermal radiation emitted by a highly absorptive substrate. In Sec. IV, we discuss the results of the study presented in this paper.

II. MODEL AND THEORETICAL FRAMEWORK

We model the three-dimensional photonic crystal as a finite inverted opal structure. Inverted opal photonic crystals are ideal for high-quality, large scale fabrication of photonic band gap materials with band gaps at micron or submicron wavelengths [24,25]. The existence of natural opals (a natural photonic crystal consisting of spherical "particles" sitting on a fcc lattice) suggested that similar artificial microstructures can be fabricated through colloidal self-assembly. The threshold for the index of refraction contrast required to obtain a full photonic band gap in opal structures is 2.8, and the opening of the gap is favored in inverted structures, i.e., structures in which the fcc spheres are made out of low-index of refraction dielectric material, while the background material presents a high index of refraction. The fabrication procedure [25], while presenting numerous experimental challenges, is principally straightforward. The initial structure, usually a close-packed face centered cubic lattice of SiO_2 spheres (direct opal), is infiltrated with high refractive index material such as Si or Ge and subsequently the original SiO_2 dielectric material is removed by chemical etching. Theoretical and experimental studies have shown that depending on the degree of infiltration, PBG materials with band gaps in the range of 5%–15% of the central frequency can be realized [18].

In our study, we consider a fully infiltrated inverted opal structure made out of silicon ($\epsilon_{Si}=11.9$). Such a structure

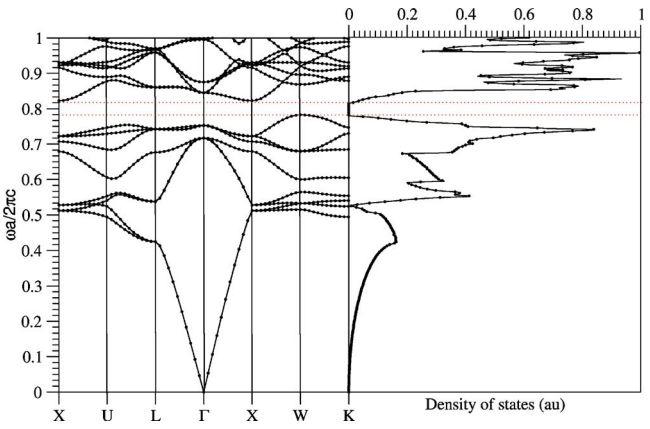

FIG. 1. (Color online) Band structure and corresponding density of states (DOS) for a close-packed fcc lattice of air spheres in silicon ($\epsilon_{Si}=11.9$) (see also Ref. [18]).

consists of close-packed fcc cubic lattice of air spheres in a high index of refraction dielectric background. In the absence of absorption and for an infinite periodic structure, the band structure and density of modes calculations reveal a relatively broad photonic band gap between the eighth and ninth bands, centered around the frequency $\omega_C=0.87\omega_0$ with a band gap width of 4.25% of the central frequency (Fig. 1) (see also Ref. [18]). For this crystal structure, we compute the transmission and the reflection coefficients of the crystal, $\mathcal{T}$ and $\mathcal{R}$, respectively, as a function of the frequency ω and the wave vector $\mathbf{k}$ of the incident wave. For a crystal with real indices of refraction (no absorption or gain), the conservation of the energy requires $\mathcal{R}+\mathcal{T}=1$. On the other hand, in the presence of absorption (corresponding to a complex index of refraction), there will be a nonzero absorption coefficient and conservation of energy requires $\mathcal{A}=1-\mathcal{R}-\mathcal{T}$. Moreover, Kirchoff's second law states that a material's thermal emittance $\mathcal{E}$ is proportional to its absorbance—and that the emittance is equal to its absorbance for a perfect blackbody thermal element. In this case, we have

$$\mathcal{E}_{\mathbf{k}}(\omega)=\mathcal{A}_{\mathbf{k}}(\omega)=1-[\mathcal{R}_{\mathbf{k}}(\omega)+\mathcal{T}_{\mathbf{k}}(\omega)], \tag{1}$$

where $\mathcal{E}_{\mathbf{k}}(\omega)$ is the ratio of the thermal optical power (Poynting's vector) emitted at the frequency ω into a spherical-angle element $d\Omega_{\mathbf{k}}$ by a unit surface area perpendicular on $\mathbf{k}$, to the power emitted by a blackbody at the same temperature, T. Then, the emittance can be obtained by simply multiplying Planck's blackbody power spectrum by the absorption coefficient [15]

$$E_{\mathbf{k}}(\omega,T)=\mathcal{E}_{\mathbf{k}}(\omega)\frac{\omega^2}{2c^2}\frac{\hbar\omega}{e^{\hbar\omega/k_BT}-1}. \tag{2}$$

As pointed out previously [15], and explicitly proved by numerical simulations of one-dimensional [27] and two-dimensional photonic crystals [28], this "indirect" method of evaluating the emittance is equivalent to the direct method that involves a quantum mechanical evaluation of the power spectrum of the elementary absorbers/emitters interacting with the photonic reservoir of modes of the periodic dielectric structure.

In evaluating the transmission, reflection and absorption coefficients for the finite inverted opal structure, we employ the numerical formalism developed in Refs. [26,29]. Based on the transfer matrix method (TMM) and on-shell techniques, the formalism is highly efficient and accurate in evaluating the optical properties of a multilayer sequence of spherical particles embedded in a homogeneous dielectric host. The principle of TMM is straightforward: the total dielectric structure is divided into small cells and the associated complex transmittance and reflectance t and r, respectively, for a given cell are evaluated. Then the fields in each cell are coupled to those of neighboring cells, and the total transfer matrix is relating the incident electric fields on the left side of the structure to the outgoing fields on the right side. The method also allows for the computation of the band structure of an infinite structure, but its major advantage is that it allows the evaluation of the transmission, reflection and absorption coefficients for fields incident on finite-thickness slabs of photonic crystal. For example, in a one-dimensional case, the $\mathcal{T}$ and $\mathcal{R}$ are equal to $|t|^2$ and $|r|^2$, respectively, where t and r are the complex transmittance and reflectance coefficients, respectively. These coefficients are linearly related to one another by a 2×2 matrix $\hat{\mathbf{M}}$, according to

$$\begin{bmatrix} 1 \\ r \end{bmatrix} = \hat{\mathbf{M}} \begin{bmatrix} t \\ 0 \end{bmatrix}, \tag{3}$$

where

$$\hat{\mathbf{M}} = \begin{bmatrix} M_{11} & M_{12} \\ M_{21} & M_{22} \end{bmatrix}. \tag{4}$$

The column vectors on each side of Eq. (3) represent the fields outside each side of the crystal. Then $t=1/M_{11}$ and $r=M_{21}/M_{11}$. This matrix $\hat{\mathbf{M}}$ can be constructed for a one-dimensional structure simply by multiplying the transfer matrices for the individual layers. For a homogeneous plate, these individual layer transfer matrices can be readily computed by taking into account the reflection and transmission at the interface at the edges of the plate with the Fresnel equations, along with the accumulated phase (and possible change in amplitude, if the index of refraction has an imaginary component) from propagating through the material. Because the phase accumulated from the wave propagating through a given layer depends on the portion of the wave vector that is perpendicular to the interfaces of the plates, the frequency ω at which the gap is centered is highly dependent on the angle of incidence of the initial radiation.

The on-shell method used by a Stefanou and co-workers [26,29] allows the evaluation of the optical response of finite number of parallel planes of spheres of differing index of refraction from the host material in which they are embedded. For a given frequency ω, the incident plane wave is expanded into spherical waves about an origin centered at one sphere, and then the scattered wave from a single sphere in one plane is calculated by satisfying the boundary conditions for Maxwell's equations at the surface of a single sphere. The scattered wave for the entire infinite plane of spheres is just the sum of the scattered waves for a single sphere expanded about a translated origin, with a phase factor corresponding to the portion of the incident wave vector that is parallel to the plane of spheres. By summing this first-order scattering of all the spheres, *except* the sphere at the origin, and then expanding the result into spherical waves about the origin, we can obtain a better approximation of the wave that is incident on the sphere at the origin. Here, the restriction that each plane of spheres has the same two-dimensional periodicity implies that the cumbersome spherical wave expansion is calculated only once per frequency, which makes this method much more numerically feasible than other approaches. By solving the boundary conditions again, with the spherical wave expansion of the incident plane wave plus this first order scattered wave, we solve for a second-order scattering of the sphere at the origin. By symmetry, all the spheres of the infinite plane have this same scattered wave. Hence, the total scattered wave for the plane is again the sum of the scattered waves for a single sphere, expanded about a translated origin, with a phase factor. The end result is then expanded into plane waves and added to the incident wave to solve for the total transmitted and reflected field. By repeating this procedure for each plane of spheres, the total field for the entire crystal is obtained.

The multiple scattering techniques and the TMM which constitute the basis of the numerical algorithms used are extremely accurate and highly efficient means to characterize the optical response of the structure considered, since the scattering matrix of each sphere can be obtained analytically. Moreover, the TMM approach is conceptually much simpler than the traditional quantum electrodynamics method of solving the nontrivial boundary conditions involved, and also not nearly as computationally intensive as the finite difference time domain (FDTD) simulations. This technique also takes into account the essentially finite nature of the structure, crucial for experimental work where often it is possible to fabricate only a few layers of crystal, and it is often necessary to account for the inherent presence of absorption that characterizes many of the dielectric materials that the photonic crystal samples are made out of.

III. NUMERICAL RESULTS

Our goal is to evaluate the emissivity of three-dimensional inverted opal photonic crystal and investigate its dependence on the angle of the incident radiation.

As depicted in Fig. 2, the fcc crystal (lattice constant a) grown along the [111] direction is modeled as a sequence … ABCABC … of parallel planes of dielectric spheres of radius r and high-dielectric constant ϵ_2 embedded in low-dielectric constant medium (ϵ_1). The individual layers of spheres A, B, C have the same periodicity in xy plane (the centers of the spheres are arranged on a triangular lattice of lattice constant $a_{xy}=a/\sqrt{2}$), but each layer is displaced to the one below by $\mathbf{d}=a(\sqrt{(2/4}, \sqrt{6/12}, \sqrt{12/6})$. In the calculations presented in this paper we have used a spherical wave expansion with a cutoff in the angular momentum of $l_{\max}=7$ and $p=37$ two-dimensional (2D) reciprocal lattice vectors in the xy plane-wave expansion. For a nonabsorbing dielectric structure, this choice of parameters provides a fractional rela-

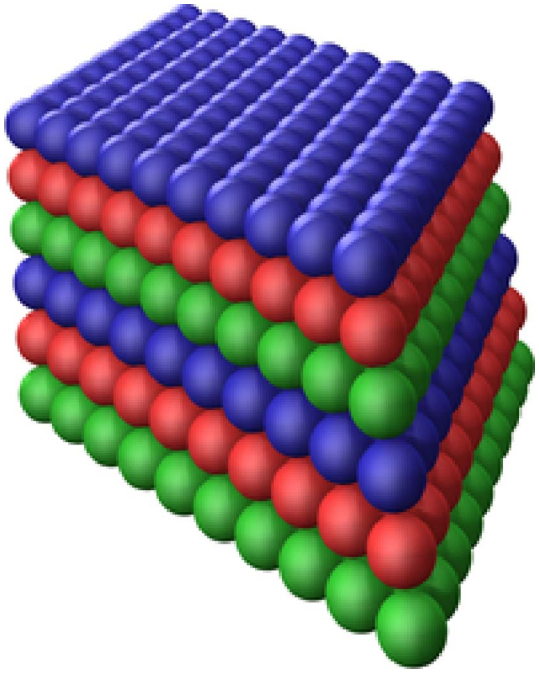

FIG. 2. (Color online) A close-packed opal structure ($r/a=\sqrt{(2)}/4$ viewed as a sequence of … ABCABC … planes grown along the [111] direction. In each plane, the high-dielectric constant spheres are embedded in a low-dielectric constant host medium (here, for simplicity, the dielectric background is assumed to be air) and are sitting on a triangular lattice of lattice constant $a_{xy}=a/\sqrt{2}$. In the numerical simulations, the structure is assumed to extend to infinity in the xy plane, but to have a finite size along the growth direction.

tive accuracy of 10^{-5} for the transmittance of an individual layer of spheres [30]. The inverted opal, shown in Fig. 3, is modeled using the same algorithm by interchanging the dielectric constants of the spheres and the embedding medium. In all the simulations, we assume that the photonic crystal sample is sitting atop a very long substrate (100 times thicker

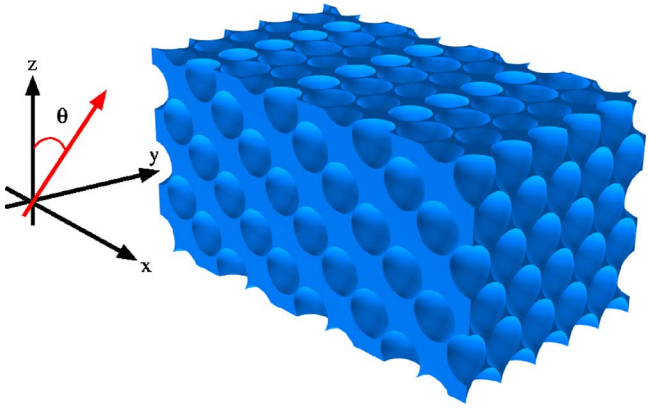

FIG. 3. (Color online) A close-packed inverted opal structure $[r/a=\sqrt{(2)}/4$ viewed as a sequence of … ABCABC … planes grown along the [111] direction. In each plane, the low-dielectric constant spheres (here, for simplicity, we assume air spheres) are embedded in a high-dielectric constant host medium and are sitting on a triangular lattice of lattice constant $a_{xy}=a/\sqrt{2}$.

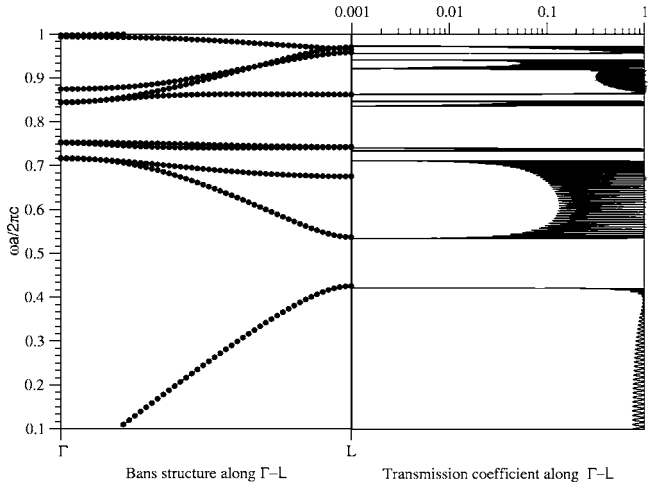

FIG. 4. Band structure and transmission coefficient for a close-packed inverted structure of air spheres in a silicon ($\epsilon=11.9$) background along the Γ-L direction. In the evaluation of the transmission coefficient, the photonic crystal is assumed to extend to infinity in the xy plane but to have a finite thickness (16 unit cells) along the z direction and we consider s-polarized incident light. The photonic crystal consists of close-packed air spheres ($\epsilon_{\text{air}}=1$) in a silicon dielectric background ($\epsilon_{\text{Si}}=11.9$).

than the total height of the photonic crystal) with dielectric constant ϵ_2 and the whole system is placed in air.

A. Transmission spectrum for nonabsorbing inverted opal structure

We begin by evaluating the transmission coefficients for a close-packed inverted opal photonic crystal. For simplicity, we considered here only the case of s-polarized incident radiation (the electric field of the incident radiation is perpendicular to the plane of incidence). As shown in Fig. 4, for incoming light along the [111] growth direction of a 16 unit cell inverted opal structure, we obtain a very good agreement with the predictions of band structure for an infinite photonic crystal (Fig. 1). The fundamental stop gap (centered around $\omega\approx 0.48\pi c/a$) and the stop gap between the eighth and the ninth bands (that includes the full photonic band gap of the crystal) correspond to strong dips in the transmission curves. The very small values of the transmission coefficient in these spectral ranges confirm that for a 16 unit cell structure the band gap effect is fully developed. Apparently, the transmission calculations show extra stop bands in the higher-order bands part of the spectral range considered. The low transmission in these spectral regions is not caused by the absence of propagating electromagnetic modes (the band structure clearly shows the existence of propagating modes in these regions) but rather than that by the inability of the incident radiation to couple to the nondegenerate photonic bands along the [111] direction of the fcc lattice. These nonoptically active bands have been thoroughly investigated theoretically [31,32] and have been experimentally observed in 2D photonic crystals [33].

As the angle of incidence is increased (see Figs. 5, 6, and 7), the frequencies that define the stop gap shift and the stop

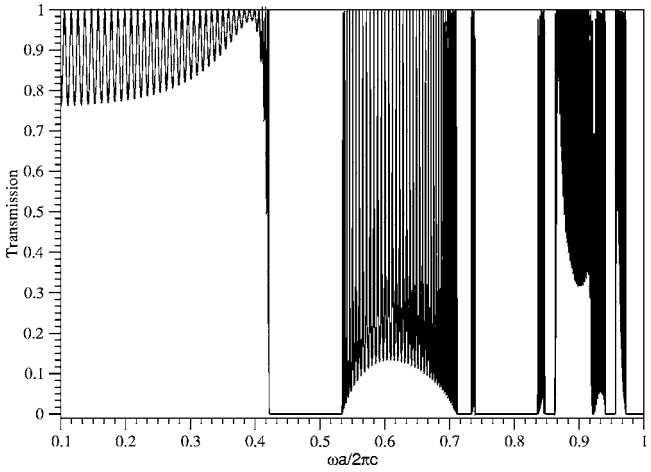

FIG. 5. Transmission spectrum for a 16 unit cell inverted opal structure for *s*-polarized incident light along the [111] direction of the underlying fcc lattice.

gaps width decreases. However, if all possible angles of incidence were explored only the stop gaps between the eighth and the ninth bands will survive and their overlap will generate the full band gap shown in Fig. 1.

B. Absorption and thermal power spectra for an inverted opal structure: Photonic crystal as active emitter

We now include the effects of absorption. For simplicity, we assume a close-packed inverted opal of "lossy" air spheres ($\epsilon_1 = 1 + 0.001i$) in silicon dielectric background ($\epsilon_2 = 11.9$). The choice of a frequency-independent absorbing medium is made for simplicity. With a frequency independent dielectric constant, it is possible to investigate the effects of absorption throughout the whole spectral range with a single numerical run and to distinguish more easily the

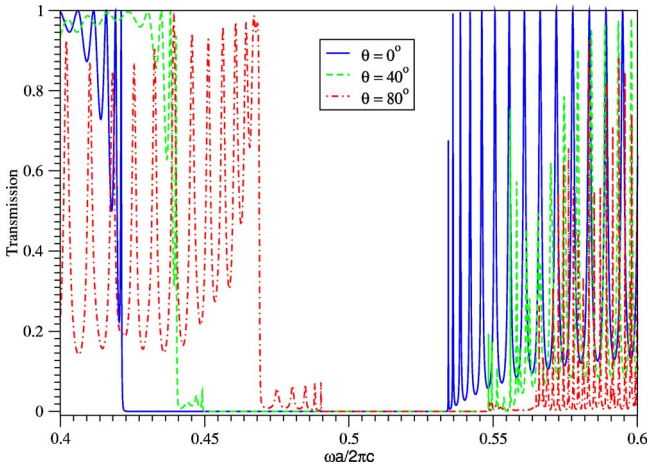

FIG. 6. (Color online) Transmission spectra for a 16 unit cell inverted opal structure on a spectral range centered around the low-frequency edge of the first stop gap, for *s*-polarized incident light with increasing angles of incidence with respect to the [111] direction (Γ-*L* direction in the reciprocal space, which is denoted by $\theta = 0$ in the figure).

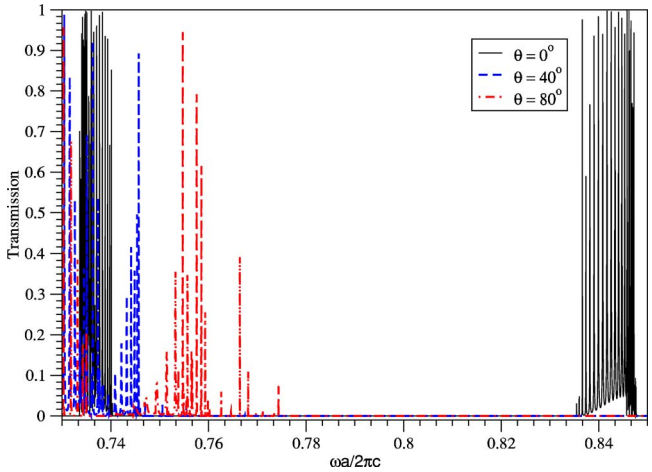

FIG. 7. (Color online) Transmission spectra for a 16 unit cell inverted opal structure on a spectral range centered around the full photonic band gap of the underlying lattice, for *s*-polarized incident light with increasing angles of incidence with respect to the [111] direction.

effects of the absorption from the effects of the dispersion of the real part of the dielectric constant [34] on the optical response of the photonic crystal sample. Experimentally, the configuration considered here can be realized by infiltrating an absorptive material (such as a gas vapor) in the voids of the inverted opal photonic crystal. The emissivity dependence on normalized frequency and polar angle for both polarizations is presented in Figs. 8, 9, and 10. Several important features are present. The absorption is strongly enhanced at the band edge location for the stop gaps along different propagating directions in the photonic structure. For given directions, the absorption almost reaches unity at the band edge resonance frequencies. This in turn implies that the emission is enhanced up to the pure blackbody limit rate at these frequencies. This observation is consistent with previous one-dimensional calculations [15,16], and recent experimental observations [22]. As noted in the previous work [15,16], around the band edge resonances, the three-

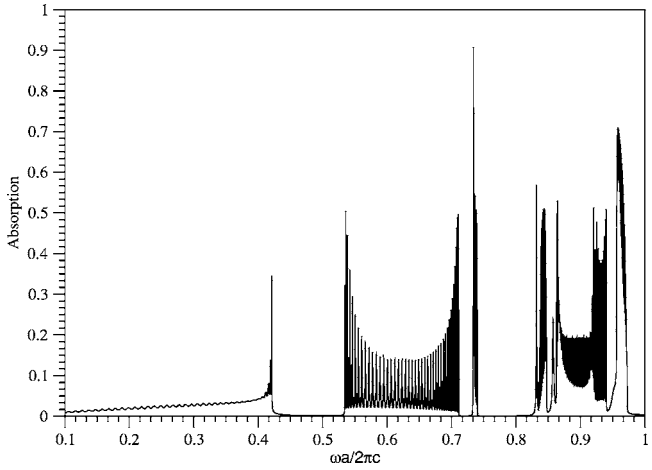

FIG. 8. Absorption spectrum for *s*-polarized incident light on a 16 unit cell inverted opal structure in the case of normal incidence.

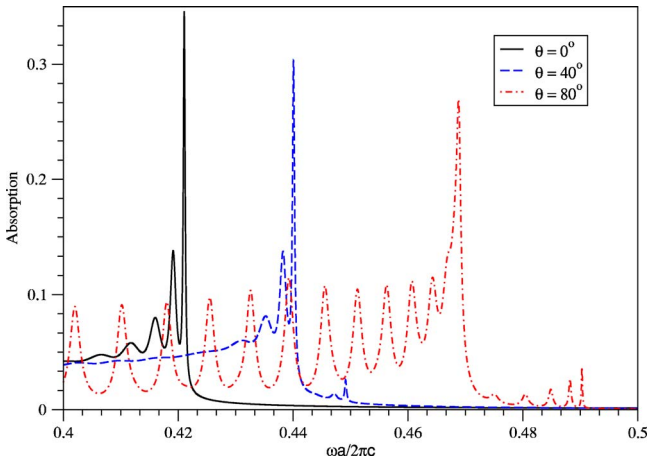

FIG. 9. (Color online) Absorption spectra for *s*-polarized incident light on a 16 unit cell inverted opal structure for different angles of incidence for a spectral region centered around the low frequency fundamental stop gap.

dimensional photonic crystal superstrate acts as an antireflective coating, allowing all incident radiations at the frequency to be absorbed—which is the definition of a blackbody. Thus, the emissivity is also enhanced considerably for given spectral ranges and well defined incident directions. This result opens a way to realize a frequency-sensitive and angle-sensitive photonic crystal absorber/emitter.

We also obtain that in the presence of the absorption the band edge location shifts and becomes not so well defined. This can be seen in Figs. 9 and 10, where we plot the evolution of the lower edge of the first stop gap and spectral region surrounding the full band gap, respectively, as the angle of incidence departure from the Γ-L direction increases. The absorption spectrum features reflect the spectral dependence of the transmission coefficient for the lossless sample, since for high transmission regions the light travels throughout the photonic crystal sample and has a better chance of being absorbed. This is best illustrated in Fig. 9,

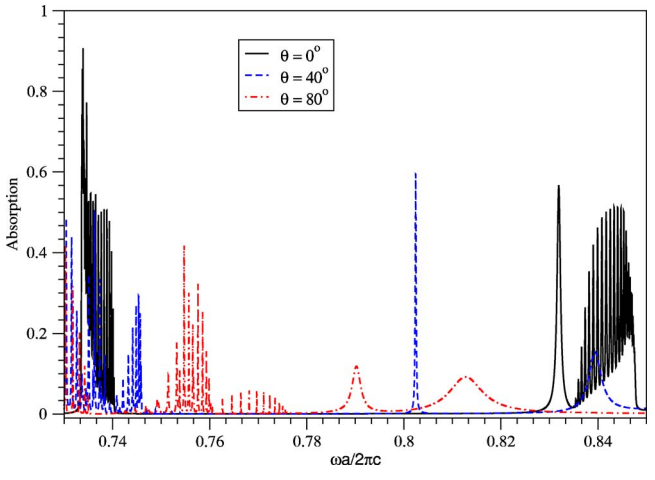

FIG. 10. (Color online) Absorption spectra for *s*-polarized incident light on a 16 unit cell inverted opal structure for different angles of incidence for a spectral region centered around the full photonic band gap of the underlying lattice.

where the absorption spectrum features follow closely the transmission spectrum of a lossless photonic crystal from Fig. 6. For a lossless photonic crystal structure, it should be noted that the reflected electromagnetic field carries with it an additional characteristic that is not presented in the reflection spectrum: the penetration depth of the reflected radiation into the photonic crystal sample. The radiation reflected penetrates in the photonic crystal on a range of 2–5 unit cells and the penetration depth is related to the imaginary part of the inverse of the Bloch wave number [35] and is strongly dependent on the incident direction and the frequency of the radiation (the exact angular and spectral dependence are determined by the topology of the photonic crystal along the incident direction considered). Therefore, due to the finite path inside the PC sample part of the radiation that would have been reflected by a large lossless sample is being absorbed. The fraction of the radiation that is absorbed is proportional to the penetration depth, and, implicitly, strongly depends on incident direction and frequency of the radiation. This mechanism is best illustrated in Fig. 10, and determines spectral features in the absorption spectrum that are complementary present in the reflection spectrum and are not visible in the transmission spectrum of a large lossless photonic crystal (see Fig. 7). Consequently, the extra features present in the absorption spectrum may be attributed to the geometrical characteristics of the photonic crystal sample. All the effects of absorption on the optical response of photonic crystals have to be carefully taken into account when designing photonic crystal structures for control of the thermal emission and absorption.

C. Absorption spectrum of an inverted opal structure: Photonic crystal as passive filter

In this section, we consider a finite inverted opal structure consisting of 16 unit cells along the [111] growth direction stacked on a highly absorptive substrate ($\epsilon = 11.9 + i$), which is 100 times thicker than the total height of the photonic crystal, so that it can be considered essentially infinitely thick. The emissivity dependence on normalized frequency and polar angle for *s*-polarized incident light is given in Figs. 11 and 12. This configuration models the experimental configuration where a lossless photonic crystal sits on top of a heated hot-plate (substrate). In this case, the photonic crystal acts as a passive filter by blocking the radiation that would normally reach the absorptive substrate and the absorption spectrum of the substrate will in fact probe the transmission spectrum of the photonic crystal coating. In the absence of the photonic crystal coating, the absorptive material interface is highly reflective (if the ambient medium is air, the reflection coefficient at this interface is around 60%). Hence, by itself, the absorptive substrate is not a very efficient absorber, even if its absorption coefficient may have a relatively large value. We note in Figs. 11 and 12 that in the spectral range corresponding to the stop gaps, the absorption is strongly inhibited. However, at the band edge frequencies (which correspond to transmission resonances in the photonic crystal), the absorption is strongly enhanced to almost unity. The photonic crystal behaves as a unidirectional planar blackbody

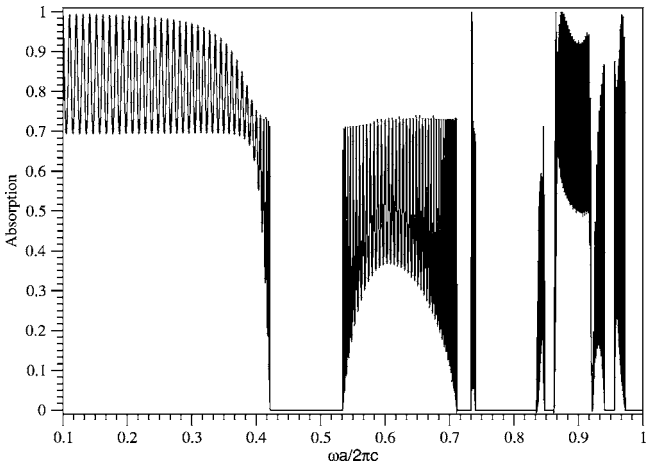

FIG. 11. Absorption spectra for *s*-polarized incident light on a 16 unit cell inverted opal structure stacked on highly absorptive ($\epsilon=11.9+i$) and very thick ($t=160a$) substrate for normal incidence along the [111] direction.

system by eliminating the index of refraction contrast presented by the substrate alone. Similar to the one-dimensional case analyzed in Ref. [15], at these select frequencies, all incident radiation tunnels through the photonic crystal into the substrate where it is eventually absorbed, and the total structure acts as a perfect absorber.

Furthermore, we have calculated the frequency-dependent and incident propagation direction-dependent emittance $\mathcal{E}_{\mathbf{k}}(\omega)$, which represents the relative power emitted for a given frequency with respect to a perfect blackbody absorber. To obtain the absolute power spectrum emitted and measured by a distant detector, we need to multiply the emittance (assumed to be equal to the absorbance) by the Planck blackbody power spectrum [see Eq. (2)]. Depending on the temperature, the maximum of a regular blackbody Planck spectrum can be made to coincide with a specific feature of the absorption spectra shown in Fig. 8. In Fig. 13, we plot

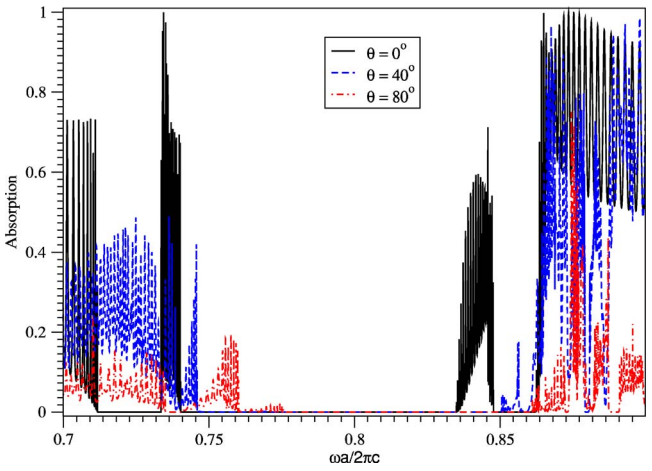

FIG. 12. (Color online) Absorption spectrum for *s*-polarized incident light on a 16 unit cell inverted opal structure stacked on highly absorptive ($\epsilon=11.9+i$) and very thick ($t=160a$) substrate for a frequency interval centered around the full photonic band gap of underlying periodic lattice for different angles of incidence.

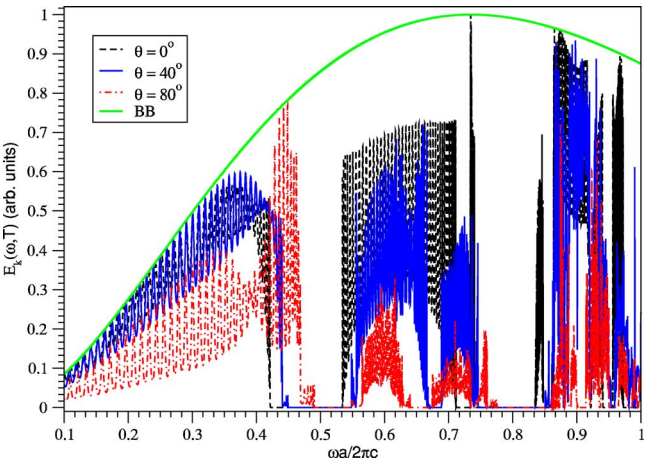

FIG. 13. (Color online) The absolute thermal power spectra for *p*-polarized incident light on a 16 unit cell inverted opal structure stacked on highly absorptive ($\epsilon=11.9+i$) and very thick ($t=160a$) substrate for different angles of incidence at $T=1873.5$ K. The temperature is chosen such that the blackbody peak aligns with the low-frequency band edge and the spectrum is normalized to the blackbody spectrum in free space.

the normalized power spectra for different directions of propagation in the photonic crystal. We chose to align the lower band edge frequency at normal incidence, $\omega=0.73\ \omega_0$ (where $\omega_0=2\pi c/a$), with the maximum of the Planck blackbody spectrum. Using the fact that the Planck's blackbody spectrum peaks at $\omega_{\max}\approx 2.82 k_B T/\hbar$, the temperature necessary to obtain this alignment is then determined by

$$k_B T = \frac{0.73}{2.82}\hbar\omega_0. \tag{5}$$

For an inverted opal with $a=2\ \mu$m, Eq. (5) yields: $T=1873.5$ K.

The results presented in Fig. 13, where we show the absolute thermal power spectra for *s*-polarized incident light on a finite inverted opal structure stacked on highly absorptive and very thick substrate for different angles of incidence also suggest an innovative way in realizing frequency and angle-selective thermal absorber/emitter. Since the band edge maxima of the absorption coefficient occur at different frequencies depending on the direction considered, by matching the blackbody emission spectrum peak with a prescribed maximum of the absorption coefficient along a specific direction, it is possible to achieve an angle-sensitive enhancement of the thermal emission/absorption of radiation. In the present configuration the effect is reduced due to the fact that the band edge falls at relatively high frequency values as compared to the frequency scale in the problem ω_0—the radiative energy density function in Eq. (2) has a maximum at $\omega_{\max}=2.82\ k_B T/\hbar$ of $\langle W(\omega_{\max},T)\rangle=1.42\ k_B^3 T^3/\hbar^2\pi^2 c^3$, and a full width at half maximum (FWHM) of $\Delta\omega_{BB}=4.25\ k_B T/\hbar$ between $\omega_1=1.16\ k_B T/\hbar$ and $\omega_2=5.41\ k_B T/\hbar$. By matching the transmission resonance frequency ($\omega_{\max}$) with the peaks of the Planck's blackbody radiation spectrum, we have $\omega_{\max}=k_B T/2.82\hbar$, and then: $\Delta\omega_{BB}=12.01\ \omega_{\max}$. Thus, the frequency selectivity, $\Delta\omega_{BB}$ (which, in turn, determines the

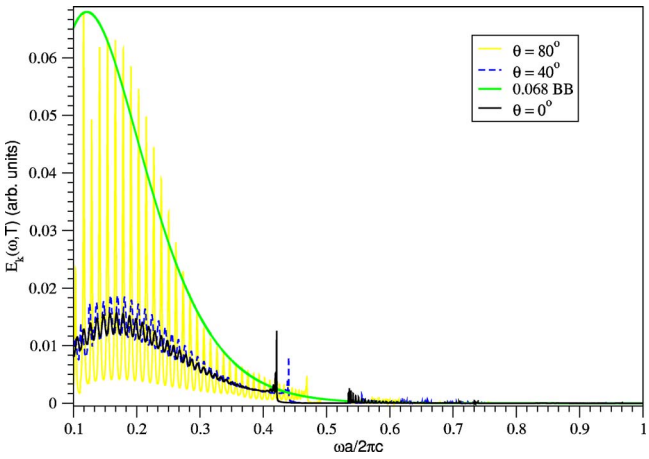

FIG. 14. (Color online) The absolute thermal power spectra for *s*-polarized incident light on a 16 unit cell inverted opal structure for different angles of incidence at $T=309$ K. The temperature is chosen such that the blackbody peak aligns with a spectral feature located in the low-frequency part of the spectrum ($\omega \approx 0.121\ \omega_0$) and the spectrum is normalized to the blackbody spectrum in free space. The figure illustrates the possibility to achieve angular selectivity for the thermal response of the photonic crystal system and the interplay between the choice of temperature, which determines the maximum of the thermal power at $\omega \approx 0.12\ \omega_0$, and the absorption coefficient of the photonic crystal, which give rise to the local maxima located around $\omega \approx 0.45\ \omega_0$. The magnitude of the blackbody thermal power spectrum has been scaled down to fit on the same plot.

angular selectivity) is directly proportional to the band edge frequency. For example, in the configuration considered in Sec. III B, let us align the peak of Planck's blackbody radiation spectrum to a spectral feature located in the low-frequency part of the spectrum ($\omega \approx 0.12\ \omega_0$, with the corresponding temperature of $T \approx 309$ K). As shown in Fig. 14, the system acquires an angular selective thermal response: the thermal radiation is preferentially emitted/absorbed at an angle of 80° with respect to the growth direction of the dielectric microstructure. However, for practical applications, the dielectric structure has to be designed such that the overall thermal response of the system has a large magnitude as well as a strong angular dependence. To this end, it is necessary not only to match the maximum of the blackbody radiation spectrum to a maximum of the absorption coefficient associated with a transmission resonance of the photonic crystal, but also to insure that these spectral features are located at relatively small values of the scaled frequency $\omega a/2\pi c$. In this case, the blackbody radiation spectrum narrows and this frequency sensitivity can be used to preferentially enhance the inherent angular selectivity of the absorption coefficient of the structure. This may be the case for photonic crystal that presents band gaps between lower index bands, such as the photonic crystals in the A-7 symmetry class [36].

IV. CONCLUSION

In summary, we have investigated the spectral and directional properties of the emission of thermal radiation of finite inverted opal photonic crystals. The physical origin of the spectral and angular dependence of the thermal emission is determined by the intricate properties of the coupling of the sources of radiation placed inside the photonic crystal and the electromagnetic mode structure inside the photonic crystal.

While a qualitative picture of the thermal emission properties of photonic crystal structures can be inferred from simulations of infinite, nonabsorbing structures (based on local density of states, group velocity, and electromagnetic field modes spatial distribution), the finite character of the dielectric microstructure and the presence of the absorptive material bring with them important changes to this picture. The frequency and angle dependent transmission resonances, the sharpness and the exact position of the band edge frequencies that define the band gap spectral range are strongly dependent on the size of the dielectric microstructure, on the structure topology, and the amount of absorption present. Our analysis shows that in the presence of the absorption into the dielectric microstructure, the transmission coefficient dependence on the frequency presents tails that enter the stop gap (where for a nonabsorbing structure no propagating modes are allowed) and the stop gap range acquires a stronger dependence on the incident propagation direction.

The precise characterization of the angular and spectral dependence of the thermal response of the photonic crystal structure analyzed in this paper can be of direct use in designing highly efficient thermal energy conversion devices. By matching the coefficient of absorption maxima to the blackbody emission spectrum pea, it is possible to achieve a highly angle-sensitive enhancement of the thermal emission/absorption of radiation. The approach that we suggest is to use angle-selective photonic-crystal based absorbers and achieve a reduction of the solid angle over which the absorber emits its energy. An angle-selective absorber has the same functionality as concentrators and could double the efficiency of a thermovoltaic energy conversion device [23].

ACKNOWLEDGMENTS

M.F. thanks Dr. Ovidiu Toader for useful discussions. Part of this work was performed at the Jet Propulsion Laboratory, California Institute of Technology, under a grant from the National Aeronautics and Space Administration. M.F. acknowledges support from the National Research Council, as well as NASA Code S, and J.D. would like to acknowledge the Horace C. Hearne Jr. Foundation.

[1] C. M. Bowden, J. P. Dowling, and H. O. Everitt, special issue of J. Opt. Soc. Am. B **10**, 279 (1993).
[2] J. W. Haus and G. Kurizki, J. Mod. Opt. **41**, 345 (1994).
[3] J. D. Joannopoulos, R. D. Meade, and J. N. Winn, *Photonic Crystals* (Princeton University Press, Princeton, 1995).
[4] E. Yablonovitch and K. M. Leung, Physica B **175**, 81 (1991).
[5] H. Sözüer and J. P. Dowling, J. Mod. Opt. **41**, 231 (1994).
[6] E. Yablonovitch, Phys. Rev. Lett. **58**, 2059 (1987).
[7] S. John, Phys. Rev. Lett. **58**, 2486 (1987).
[8] A. Kaufman, G. Kurizki, and B. Sherman. J. Mod. Opt. **41**, 353 (1994); S. John and T. Quang, Phys. Rev. A **50**, 1764 (1994); M. Lewenstein, J. Zakrzewski, and T. W. Mossberg. *ibid.* **38**, 808 (1988); Y. Yang and S. Y. Zhu, *ibid.* **62**, 013805 (2000).
[9] S. Y. Zhu, H. Chen, and H. Huang, Phys. Rev. Lett. **79**, 205 (1997); T. Quang, M. Woldeyohannes, S. John, and G. S. Agarwal, *ibid.* **79**, 5238 (1997).
[10] S. John and T. Quang, Phys. Rev. Lett. **78**, 1888 (1997).
[11] O. Painter *et al.*, Science **284**, 1819 (1999).
[12] M. Imada *et al.*, Appl. Phys. Lett. **75**, 316 (1999).
[13] M. Florescu and S. John, Phys. Rev. A **64**, 033801 (2001).
[14] S. John and M. Florescu, J. Opt. Soc. Am. A **3**, S103 (2001); M. Florescu and S. John, Phys. Rev. A **69**, 053810 (2004).
[15] C. M. Cornelius and J. P. Dowling, Phys. Rev. A **59**, 4736 (1999).
[16] A. J. Stimpson and J. P. Dowling, "Thermal emissivity of 3D photonic band-gap structures," presented at the *Optical Society of American Annual Meeting*, Long Beach, CA, 2001.
[17] S. Y. Lin, J. Moreno, and J. G. Fleming, Appl. Phys. Lett. **83**, 380 (2003).
[18] K. Busch and S. John, Phys. Rev. E **58**, 3896 (1998).
[19] M. M. Sigalas, C. T. Chan, K. M. Ho, and C. M. Soukoulis, Phys. Rev. B **52**, 11744 (1995).
[20] S. Fan, P. R. Villeneuve, and J. D. Joannopoulos, Phys. Rev. B **54**, 11245 (1996).
[21] M. U. Pralle *et al.*, Appl. Phys. Lett. **81** 4685 (2002).
[22] S. Y. Lin, J. G. Fleming, E. Chow, J. Bur, K. K Choi, and A. Goldberg, Phys. Rev. B **62**, R2243 (2000); J. G. Fleming, S. Y. Lin, I. El-Kady, R. Biswas, and K. M. Ho, Nature (London) **417**, 52 (2002).
[23] N.-P. Harder and P. Würfel, Semicond. Sci. Technol. **18**, S151 (2003).
[24] J. E. G. Wijnhoven and W. I. Wos, Science **281**, 802 (1998).
[25] A. Blanco *et al.*, Nature (London) **405**, 437 (2000).
[26] N. Stefanou, V. Yannopapas, and A. Modinos, Comput. Phys. Commun. **113**, 49 (1998).
[27] P. Pigeat, D. Rouxel, and B. Weber, Phys. Rev. B **57**, 9293 (1998).
[28] C. Luo, A. Narayanaswamy, G. Chen, and J. D. Joannopoulos, Phys. Rev. Lett. **93**, 213905 (2004).
[29] N. S. Stefanou, V. Yannapapas, and A. Modinos, Comput. Phys. Commun. **132**, 189 (2000).
[30] V. Yannopapas, N. Stefanou, and A. Modinos, Phys. Rev. Lett. **86**, 4811 (2001); Z. L. Wang, C. T. Chan, W. Y. Zhang, Z. Chen, N. B. Ming, and P. Sheng, Phys. Rev. E **67**, 016612 (2003).
[31] N. Stefanou, V. Karathanos, and A. Modinos, J. Phys.: Condens. Matter **4**, 7389 (1992).
[32] Z. L. Wang, C. T. Chan, W. Y. Zhang, Z. Chen, N. B. Ming, and P. Sheng, Phys. Rev. E **67**, 016612 (2003).
[33] W. M. Robertson, G. Arjavalingam, R. D. Meade, K. D. Brommer, A. M. Rappe, and J. D. Joannopoulos, Phys. Rev. Lett. **68**, 2023 (1992).
[34] O. Toader and S. John, Phys. Rev. E **70**, 046605 (2004).
[35] Y. Fink *et al.*, Science **282**, 1679 (1998); D. L. C. Chan, E. Lidorikis, and J. D. Joannopoulos, Phys. Rev. E **71**, 056602 (2005).
[36] C. T. Chan, S. Datta, K.-M. Ho, and C. M. Soukoulis, Phys. Rev. B **50**, 1988 (1994).